ISSN 0020-1685, Inorganic Materials, 2020, Vol. 56, No. 4, pp. 374–381. © Pleiades Publishing, Ltd., 2020.
Russian Text © The Author(s), 2020, published in Neorganicheskie Materialy, 2020, Vol. 56, No. 4, pp. 393–401.

Electrical Properties of Thin In_2O_3/C Films

I. V. Babkina[a], M. N. Volochaev[b], O. V. Zhilova[a], Yu. E. Kalinin[a], V. A. Makagonov[a, *], S. Yu. Pankov[a], and A. V. Sitnikov[a]

[a] *Voronezh State Technical University, Moskovskii pr. 14, Voronezh, 394026 Russia*
[b] *Kirensky Institute of Physics, Krasnoyarsk Scientific Center Federal Research Center, Siberian Branch, Russian Academy of Sciences, Akademgorodok 50/38, Krasnoyarsk, 660036 Russia*
**e-mail: vlad_makagonov@mail.ru*

Received March 21, 2019; revised September 12, 2019; accepted October 2, 2019

Abstract—We have studied the structure and electrical properties of thin films based on the In_2O_3 semiconductor and carbon, grown by atomic layer deposition using ion-beam sputtering. The structure of the resultant materials, formed during layer-by-layer growth of island layers, is made up of nanocrystalline In_2O_3 granules distributed at random over amorphous carbon. The electrical transport properties of the In_2O_3/C thin films depend on their thickness. In the temperature range 80–300 K, the dominant electrical transport mechanism in the In_2O_3/C thin films of thickness $h < 70$ nm sequentially changes from variable range hopping between localized states in a narrow energy band near the Fermi level (between 80 and 120 K) to nearest neighbor hopping (between 120 and 250 K) and then to variable range hopping between localized states in the conduction band tail (between 250 and 300 K). The films of thickness $h > 70$ nm undergo a change from conduction associated with strong carrier localization to that due to the presence of percolation clusters formed by In_2O_3 nanocrystals, which shows up as a linear temperature dependence of conductivity, with a negative temperature coefficient.

Keywords: amorphous and crystalline structures, electrical resistance, heat treatment
DOI: 10.1134/S0020168520040019

INTRODUCTION

Thin indium oxide (In_2O_3) films are *n*-type semiconductors with a band gap from 3.55 to 3.75 eV. They offer high optical transmission, high electrical conductivity, and excellent luminescence, which allows them to be used in transparent electronics [1], light emitting diodes [2], solar cells [3], gas sensors [4, 5], and other electronic devices.

In recent years, thin films of oxide semiconductors, including indium oxide, have been proposed for use as thin film transistor (TFT) channels [6–8]. However, the unstable and nondurable nature of the performance characteristics of semiconductors and related solid solutions in monolayer TFT channels, due to the effect of various factors (temperature, shear stress, and illuminance), requires a search for new methods of stabilizing their parameters. Instability of many electrical parameters is caused by oxygen vacancies [9]. At the same time, charge transport in transparent oxide semiconductors is known to be ensured by oxygen-related defects and, hence, the oxygen vacancy concentration determines the electrical properties of the oxide semiconductors. Thus, one has to choose between operation stability and degradation of performance characteristics. Moreover, the materials currently used to fabricate TFT channels do not meet requirements imposed on them in terms of operation speed, switching time, and carrier mobility.

One approach for resolving this problem is to fabricate two-phase nanocomposites or multilayer channel structures with high carrier mobility and high stability of their performance characteristics. The binary systems studied to date include ZnO–SnO_2, ZnO–In_2O_3, and others [10–13]. Note that the electrical and optical properties of two-phase oxide semiconductors are significantly inferior to those of pure indium oxide, but they are more stable.

To stabilize a nanocrystalline structure of indium oxide, wide use is made of doping with a variety of impurities [14, 15]. Carbon is one of the most interesting dopants for In_2O_3. It is also worth noting that the high cost of indium, necessary for the manufacture of widely used thin indium oxide films, also stimulates basic and applied research aimed at replacing it.

In this paper, we report an experimental study of the structure of heterogeneous thin In_2O_3/C films and examine its effect on the electrical properties of the films.

EXPERIMENTAL

Thin $(In_2O_3/C)_{74}$ films were grown by atomic layer deposition of In_2O_3 and C using ion-beam sputtering in a 99.998%-pure argon atmosphere at a pressure of 7×10^{-2} Pa as described by Rylkov et al. [16]. Graphite (C) and ceramic In_2O_3 targets were secured on water-cooled copper plates 280 × 80 mm in dimensions and placed in different positions in a vacuum chamber. To ensure layer-by-layer deposition, a substrate was translated from one sputtering position to another by rotating a substrate holder around the axis of the sputtering chamber at a rate of 0.13 rpm. Films were grown on (100)-oriented single-crystal silicon substrates for structural characterization and on ST-50 glass-ceramic substrates for electrical transport measurements. During the sputter deposition process, the substrates were maintained at room temperature. To obtain different thicknesses of In_2O_3 and C layers in a single sputter deposition process, *V*-shaped screens were placed between the targets and the substrate holder. In one sputter deposition cycle, four glass-ceramic plates 60 × 48 × 0.6 mm in dimensions were used as substrates, which were arranged in the form of a stripe 240 × 80 mm in dimensions at a distance of ~70 mm. The long axes of the substrate and target coincided. The use of the *V*-shaped screens and the coaxial arrangement of the target and substrate allowed films with different thicknesses of bilayers along the length of the substrate to be produced in a single deposition cycle.

To estimate the thickness of the layers, separate In_2O_3 and C films were first grown by sputter deposition at previously chosen process parameters. Before sputter deposition, we set the process parameters previously chosen for the growth of a multilayer structure. After that, the target chosen was sputtered. After a prolonged film growth process (typically for several hours) on a substrate rotating at a preset speed, we measured the thickness of the film in different regions using an MII-4 interferometer. The points at which the thickness was measured were fixed relative to the arrangement of the substrate and target. The measured thicknesses of the film were fitted as functions of the distance to the edge of the substrate. From the known sputtering time and the time per revolution of the substrate holder, we calculated the thickness of the film grown during one cycle of substrate translation through the material deposition zone. In a similar way, we determined the thickness of one layer of the second phase in the multilayer structure. The number of deposition cycles determined the number of In_2O_3/C bilayers. We performed 74 deposition cycles, which allowed us to obtain 75 thin films 28 to 138 nm in thickness, corresponding to equivalent thicknesses of In_2O_3/C bilayers from 0.38 to 1.9 nm. It is worth noting that the equivalent monolayer thickness thus obtained does not take into account the possibility of island growth; that is, this is the thickness of a thin film grown during one revolution of the substrate holder provided that the film is continuous.

The structure and phase composition of the samples thus obtained were studied by X-ray diffraction on a Bruker D2 Phaser diffractometer ($\lambda_{Cu K_{\alpha 1}} = 1.54$ Å) using DIFFRAC.EVA 3.0 software and the ICDD PDF database (Release 2012). Cross-sectional transmission electron microscopy (TEM) images and electron diffraction patterns were obtained on a Hitachi HT7700 microscope at an accelerating voltage of 100 kV (W source) at the Kirensky Institute of Physics, Krasnoyarsk Scientific Center Federal Research Center, Siberian Branch, Russian Academy of Sciences. Specimens were prepared using a focused ion beam system (Hitachi FB2100 single-beam FIB) at an accelerating voltage of 40 kV. The thickness of the specimens thus prepared was ~40–50 nm. To prevent Ga^+ beam etching, an amorphous Ge layer was grown on the surface of the thin $(In_2O_3/C)_{74}$ films by thermal evaporation.

Resistivity and thermoelectric power were measured as described elsewhere [17].

RESULTS AND DISCUSSION

Structure of the samples. Analysis of X-ray diffraction patterns of the In_2O_3 and C thin films grown by sputter deposition on a rotating substrate (Fig. 1) indicated that the In_2O_3 films were polycrystalline and that the carbon films had an amorphous structure [18, 19]. X-ray diffraction data for the $(In_2O_3/C)_{74}$ films demonstrated that all of the samples studied contained a considerable amount of an X-ray amorphous phase. A crystalline component in the form of diffraction peaks was most pronounced in the films more than 80 nm in thickness (Fig. 2a) and was identified as an In_2O_3 phase with a cubic crystal lattice (sp. gr. $Ia\bar{3}$). The average crystallite (coherent scattering domain) size was evaluated using the Scherrer formula,

$$D = \frac{0.89\lambda}{b\cos\theta}, \quad (1)$$

where λ is the X-ray wavelength (1.54 Å for $CuK_{\alpha 1}$ radiation), b is the full width at half maximum of the reflection, and θ is the Bragg angle, and was determined to be 19 and 12 nm for the 90- and 121-nm-thick samples, respectively [18]. These In_2O_3 crystallite sizes considerably exceed the corresponding equivalent bilayer thicknesses calculated for the samples in question. Thus, no extended In_2O_3 or C layers were formed at the equivalent bilayer thicknesses indicated, so the structure of the $(In_2O_3/C)_{74}$ thin films can be thought of as a composite consisting of two phases: In_2O_3 nanocrystals and amorphous carbon regions. Analysis of the X-ray diffraction patterns at small diffraction angles confirmed that none of the $(In_2O_3/C)_{74}$ thin films studied in this work had a lay-

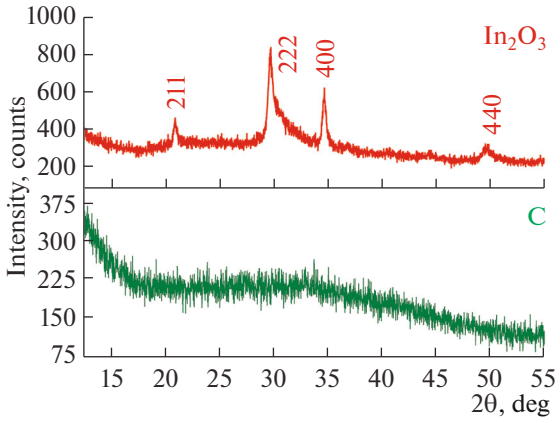

Fig. 1. X-ray diffraction patterns of the as-grown thin In_2O_3 and C films.

ered structure, as was evidenced by the absence of diffraction peaks (Fig. 2b).

To ascertain that the obtained system did not have a multilayer structure, we examined cross sections of the samples by TEM. The results supported the above conclusion that the thin films had a nanocrystalline structure (Fig. 3a) and confirmed that preliminary measurements with an MII-4 interferometer provided accurate film thicknesses. Electron diffraction also indicated the presence of crystalline In_2O_3 and amorphous carbon. The presence of the latter was evidenced by a broad halo (Fig. 3b).

Since the $(In_2O_3/C)_{74}$ thin films under study are composites, their electrical transport properties would be expected to depend primarily not on the equivalent bilayer thickness but on the total film thickness.

Low-temperature electrical properties of the $(In_2O_3/C)_{74}$ films. To assess the effect of carbon on the electrical properties of the $(In_2O_3/C)_{74}$ films under study, we measured their room-temperature resistivity and thermoelectric power (Fig. 4). The addition of carbon leads to an increase in the resistivity of the $(In_2O_3/C)_{74}$ films by almost one order of magnitude in comparison with pure In_2O_3 at any film thickness. At the same time, the resistivity of the $(In_2O_3/C)_{74}$ films remains lower than that of pure carbon films and decreases with increasing film thickness: from 2.5 Ω cm at a film thickness of 30 nm to 4×10^{-3} Ω cm at a film thickness of 135 nm (Fig. 4a). The thermoelectric power of the $(In_2O_3/C)_{74}$ films also decreases with increasing film thickness: from 75 μV/K at a film thickness of 30 nm to 28 μV/K at a film thickness of 130 nm (Fig. 4b). Their thermoelectric power is negative, pointing to *n*-type conductivity.

Analysis of the present results shows that the $(In_2O_3/C)_{74}$ films consist of island layers of nanocrystalline In_2O_3 and amorphous carbon over the entire range of film thicknesses studied, which is equivalent to the formation of a two-phase system (Fig. 3). In this case, for $h < 70$ nm the islands of the individual phases are distributed at random over the bulk of the $(In_2O_3/C)_{74}$ thin film, and its electrical conductivity is determined by the ratio of the concentration of In_2O_3 (higher conductivity phase) (Fig. 4a, curve *2*) to that of carbon (lower conductivity phase) (Fig. 4a, curve *1*). As the film thickness increases to $h > 70$ nm, the island size in the In_2O_3 and carbon layers rises and the In_2O_3 crystallites come in contact with each other to form a quasi-two-dimensional percolation cluster, which leads to a reduction in the resistivity of the film (Fig. 4a, curve *3*). In other words, if $h < 70$ nm and the two-phase system under consideration contains carbon islands, there are conditions for strong interfacial localization in the multilayer semiconductor structure in the presence of a chaotic potential due to randomly distributed lumped charges in the space charge region [20]. For $h > 70$ nm, electrical conductivity is deter-

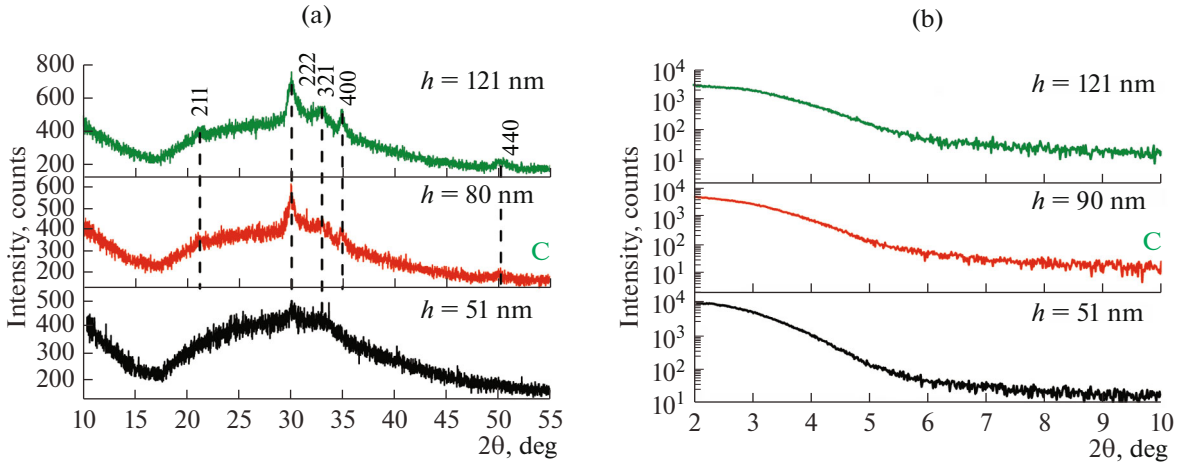

Fig. 2. X-ray diffraction patterns of the $(In_2O_3/C)_{74}$ thin films differing in thickness.

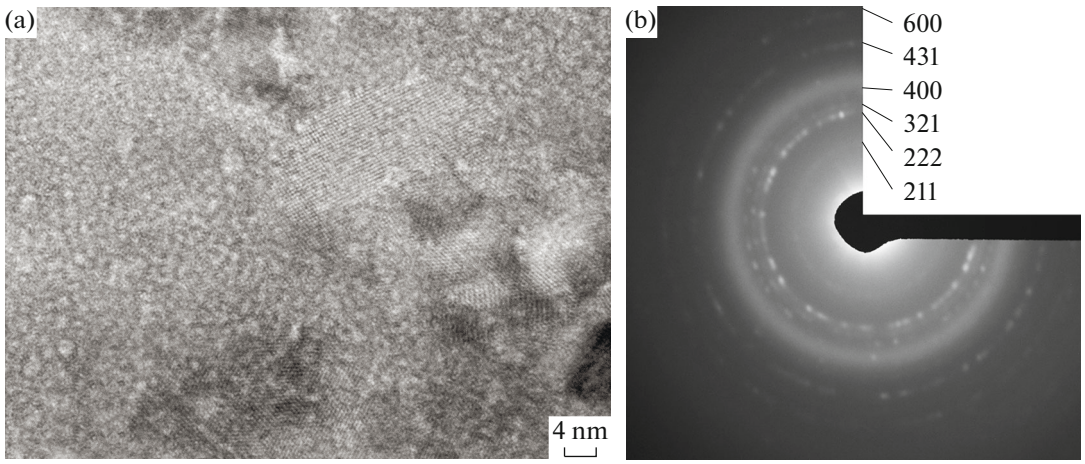

Fig. 3. (a) Cross-sectional TEM image of thin films and (b) electron diffraction pattern of $(In_2O_3/C)_{74}$ (h = 132 nm).

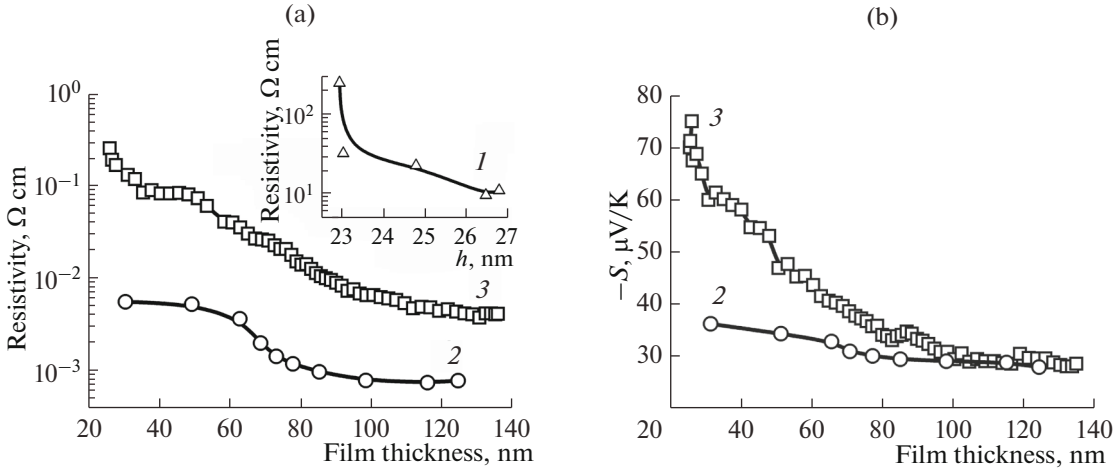

Fig. 4. Room-temperature (a) resistivity and (b) thermoelectric power as functions of film thickness for the (*1*) C, (*2*) In_2O_3, and (*3*) $(In_2O_3/C)_{74}$ thin films.

mined by the conductivity of the percolation clusters formed by the In_2O_3 crystallites. Because of this, conduction mechanisms will be analyzed here separately for the thin films with $h < 70$ nm and the films with $h > 70$ nm.

To identify the dominant electrical transport mechanisms in our samples, we examined temperature dependences of resistivity, $\rho(T)$, in the range from 80 to 300 K (Fig. 5). The $\rho(T)$ data obtained for the $(In_2O_3/C)_{74}$ films of thickness h = 43 and 65 nm were represented as plots of ln ρ against $1/T^n$ (where n = 1/4, 1/2, or 1). It was shown that, in the temperature range from 80 to 120 K, the $\rho(T)$ data represented as plots of ln ρ against $1/T^{1/4}$ are well described by a straight line (Fig. 6a), pointing to variable range carrier hopping conduction between localized states lying in a narrow energy band near the Fermi level [21]. According to Mott and Davis [21], electrical conductivity is then given by

$$\sigma = e^2 R^2 \nu_{ph} g \exp\left(-\frac{B}{T}\right)^{1/4}, \quad (2)$$

where

$$B = \frac{16}{a^3 k g(E_F)}, \quad (3)$$

$$R = \left[\frac{3}{2\pi a g(E_F) k T}\right]^{1/4}, \quad (4)$$

e is the electronic charge, R is the average hop distance, ν_{ph} is a factor of the phonon interaction spec-

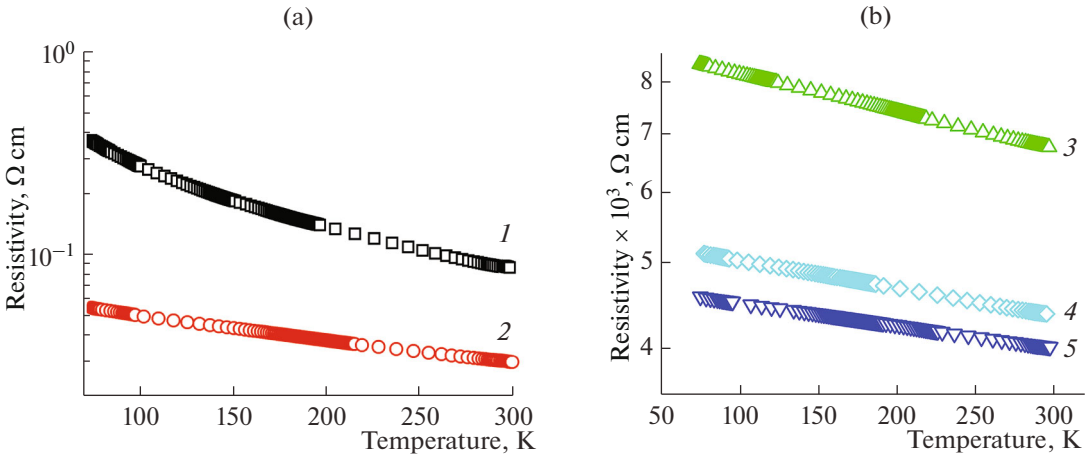

Fig. 5. Temperature dependences of resistivity for the $(In_2O_3/C)_{74}$ thin films differing in thickness: h = (*1*) 43, (*2*) 65, (*3*) 97, (*4*) 119, and (*5*) 135 nm.

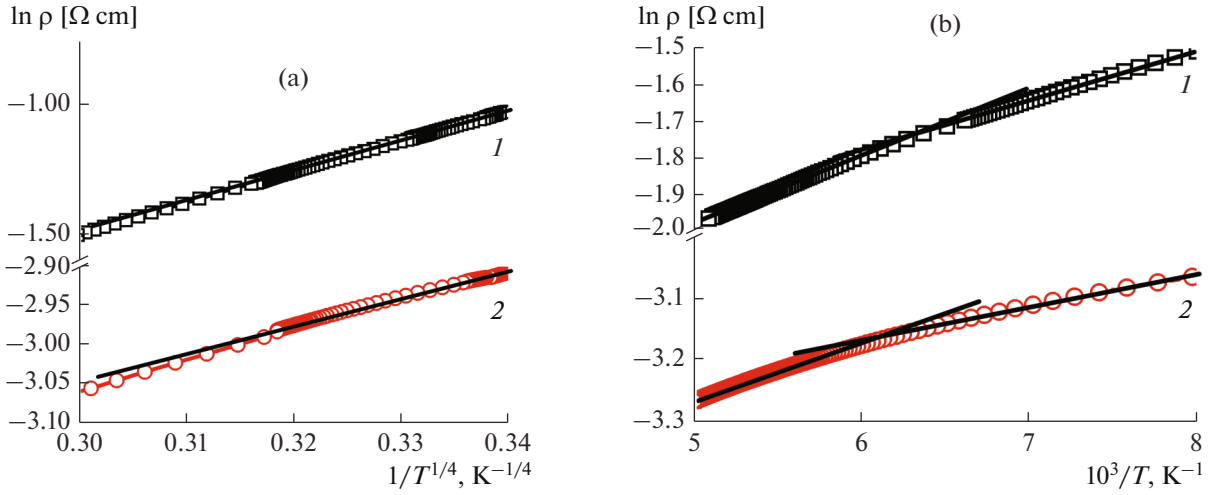

Fig. 6. Plots of (a) lnρ against $T^{-1/4}$ and (b) lnρ against $10^3/T$ for the $(In_2O_3/C)_{74}$ thin films differing in thickness: h = (*1*) 43 and (*2*) 65 nm.

trum, T is the absolute temperature, $g(E_F)$ is the Fermi level density of states, a is the localization radius of the electron wave function, and k is Boltzmann's constant.

From the data in Fig. 6a, we determined the parameter B in Eq. (2). Assuming that the charge transport process is limited by hops between dangling indium bonds, in evaluating the density of localized states we take the localization radius to be equal to the average crystallite size of In_2O_3: ≈12 nm. The Fermi level density of states estimated for the 43- and 65-nm-thick $(In_2O_3/C)_{74}$ films using relations (2)–(4) is given in Table 1. It is seen that, with increasing $(In_2O_3/C)_{74}$ film thickness, $g(E_F)$ approaches the level characteristic of the In_2O_3 films: 10^{20} to 10^{21} eV^{-1} cm^{-3} [22].

In the range from 120 to 250 K, the temperature dependences of resistivity are well described by the nearest neighbor hopping conduction model [21], according to which the following equality should be met:

$$\rho = \rho_1 \exp\left(-\frac{W_{NNH}}{kT}\right). \quad (5)$$

Table 1. Parameters of the $(In_2O_3/C)_{74}$ thin films evaluated in different models: variable range electron hopping conduction between localized states lying in a narrow energy band near the Fermi level (80–120 K), nearest neighbor hopping conduction (120–250 K), and hopping between localized states in the conduction band tail (250–300 K)

h, nm	$g(E_F)$, eV^{-1} cm^{-3}	W_{NNH}, eV	R_0, nm	E_a, eV
43	5.75×10^{18}	0.013	14.7	0.058
65	8.63×10^{20}	0.015	3.8	0.029

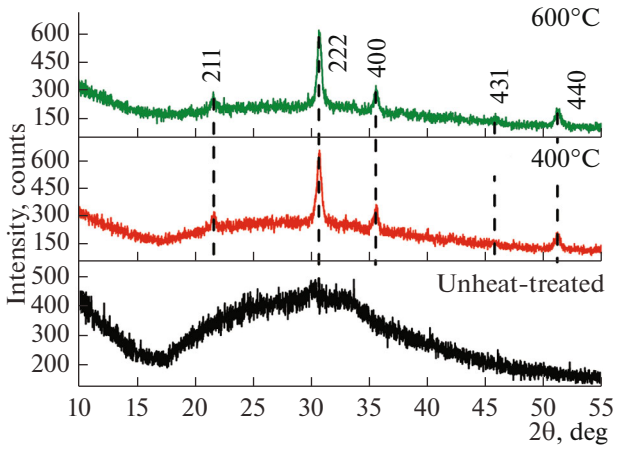

Fig. 7. X-ray diffraction patterns of the 50-nm-thick $(In_2O_3/C)_{74}$ thin films before and after heat treatment for 30 min at different temperatures.

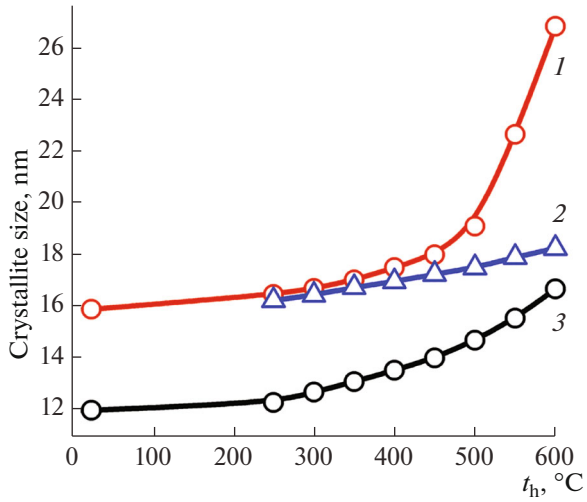

Fig. 8. Average In_2O_3 crystallite size as a function of heat treatment temperature for thin films of In_2O_3 (*1*) and $(In_2O_3/C)_{74}$ with $h = 51$ (*2*) and 121 nm (*3*).

Here W_{NNH} is the activation energy for nearest neighbor hopping:

$$W_{NNH} = \frac{3}{4\pi R_0^3 g(E_F)}, \quad (6)$$

where R_0 is the average nearest neighbor distance.

Using Eqs. (5) and (6) and taking into account the $g(E_F)$ value obtained above, we estimated W_{NNH} and R_0 from the low-temperature data in Fig. 6b. The results for the $(In_2O_3/C)_{74}$ thin films are presented in Table 1.

In the temperature range 250–300 K, the resistivity data in the form of plots of ln ρ against $10^3/T$ also have linear portions (Fig. 6b). According to Mott and Davis [21], the following relation is then valid:

$$\rho = \rho_0 \exp\left(-\frac{E_a}{2kT}\right), \quad (7)$$

where E_a is the activation energy for electrical conduction. Using (7), we calculated the activation energy for conduction (Table 1).

The experimental temperature-dependent resistivity data for the $(In_2O_3/C)_{74}$ films of thickness $h > 70$ nm, corresponding to the formation of In_2O_3 percolation clusters, are well represented by straight lines in plots of ρ against T (Fig. 5b). In this case, the temperature dependence of resistivity is similar to the $\rho(T)$ for amorphous metal–metalloid metallic alloys [23], where the contribution of phonon carrier scattering to the $\rho(T)$ behavior of the material is small. On the other hand, the negative temperature coefficient of resistivity can be due to a transition from strong carrier localization in the case of films consisting of island layers with $h < 70$ nm to weak localization at $h > 70$ nm, where the decrease in resistivity is commonly attributed to quantum interference of the wave functions of noninteracting electrons and an increased role of interelectron interaction [24].

Note that linear temperature variation of resistivity is of great practical importance in designing temperature sensors and is observed as well in thin films of carbon nanotubes [25].

Effect of heat treatment on the structure of $(In_2O_3/C)_{74}$ films. To assess the effect of heat treatment on the structural stability of the $(In_2O_3/C)_{74}$ thin films, we carried out stepwise annealing under vacuum ($p < 70$ Pa) for 30 min at temperatures t_h from 250 to 600°C at 50°C intervals. The carbon-free In_2O_3 thin films were heat-treated under similar conditions. The heat treatment increased the average crystallite size of In_2O_3 in both the carbon-free In_2O_3 thin films and the $(In_2O_3/C)_{74}$ films, as was evidenced by the observed increase in the intensity of the diffraction peaks of the In_2O_3 phase and the decrease in their width, as well as by the decrease in the intensity of the halo due to the X-ray amorphous component (Fig. 7). Moreover, raising the annealing temperature was accompanied by an increase in the average crystallite size of In_2O_3 (Fig. 8). A somewhat surprising result is that the crystallite size decreases with increasing film thickness (Fig. 8, curves *2*, *3*), which is attributable to the larger thickness of the carbon layers in the thicker films.

Besides, the data in Fig. 8 lead us to conclude that the effect of temperature on the growth of the In_2O_3 crystallites in the $(In_2O_3/C)_{74}$ films during the recrystallization process is considerably weaker than that in the In_2O_3 films. This is especially so for $t_h > 450$°C, where the most active growth of the average crystallite size in the pure In_2O_3 films begins (Fig. 8, curve *1*) [26].

Thus, the data obtained by heat-treating the $(In_2O_3/C)_{74}$ thin films under vacuum at temperatures no higher than 600°C demonstrates that the effect of

temperature on the recrystallization process in these films is considerably weaker than that in the case of the pure In_2O_3 films.

CONCLUSIONS

Atomic layer deposition of In_2O_3 and C using ion-beam sputtering produces a composite film consisting of two phases: In_2O_3 nanocrystals and amorphous carbon. In the temperature range 80–300 K, the dominant electrical transport mechanism in the $(In_2O_3/C)_{74}$ thin films of thickness $h < 70$ nm sequentially changes from Mott's variable range hopping to nearest neighbor hopping and then to variable range hopping between localized states in the conduction band tail near room temperature. The resistivity of the $(In_2O_3/C)_{74}$ films of thickness $h > 70$ nm varies linearly in the temperature range from 80 to 300 K, with a negative temperature coefficient, which is attributable to the presence of percolation clusters formed by In_2O_3 nanocrystals.

Heat treatment of the $(In_2O_3/C)_{74}$ thin films under vacuum at temperatures no higher than 600°C leads to recrystallization and an increase in the average crystallite size of In_2O_3, but the effect of temperature on the recrystallization process is considerably weaker than that in the case of the pure In_2O_3 films.

FUNDING

This work was supported by the Russian Federation Ministry of Science and Higher Education (state research target, project no. 3.1867, 2017/4.6).

REFERENCES

1. Rakesh, A., Sharma, N., Maheshwar, Sh., and Sharon, M., Transparent conducting oxide films for various applications: a review, *Rev. Adv. Mater. Sci.,* 2018, vol. 53, no. 1, pp. 79–89. https://doi.org/10.1515/rams-2018-0006
2. Morales-Masis, M., De Wolf, S., Woods-Robinson, R., Ager, J.W., and Ballif, C., Transparent electrodes for efficient optoelectronics, *Adv. Electron. Mater.,* 2017, vol. 3, no. 5, paper 1 600 529. https://doi.org/10.1002/aelm.201600529
3. Ramanujam, J., Verma, A., Gonzalez-Diaz, B., and Guerrero-Lemus, R., Inorganic photovoltaics – planar and nanostructured devices, *Prog. Mater. Sci.,* 2016, vol. 82, pp. 294–404. https://doi.org/10.1016/j.pmatsci.2016.03.005
4. Korotcenkov, G., Brinzari, V., and Cho, B.K., In_2O_3- and SnO_2-based thin film ozone sensors: fundamentals, *J. Sens.,* 2016, paper 3 816 094. https://doi.org/10.1155/2016/3816094
5. Derek, M.R., Sheikh, A.A., and Patricia, M.A., Nanoscale metal oxide-based heterojunctions for gas sensing: a review, *Sens. Actuators, B,* 2014, vol. 204, pp. 250–272. https://doi.org/10.1016/j.snb.2014.07.074
6. Sanctis, S., Krausmann, J., and Guhl, C., Stacked indium oxide/zinc oxide heterostructures as semiconductors in thin film transistor devices: a case study using atomic layer deposition, *J. Mater. Chem.,* 2018, vol. 6, pp. 464–472. https://doi.org/10.1039/C7TC03724D
7. Park, J.W., So, H.S., Lee, H.M., Kim, H.J., Kim, H.K., and Lee, H., Transition from a nanocrystalline phase to an amorphous phase in In–Si–O thin films: the correlation between the microstructure and the optical properties, *J. Appl. Phys.,* 2015, vol. 117, paper 155 305. https://doi.org/10.1063/1.4918658/
8. Mitoma, N., Aikawa, S., Gao, X., Kizu, T., Shimizu, M., Lin, M.F., Nabatame, T., and Tsukagoshi, T., Stable amorphous In_2O_3-based thin-film transistors by incorporating SiO_2 to suppress oxygen vacancies, *Appl. Phys. Lett.,* 2014, vol. 104, paper 102 103. https://doi.org/10.1063/1.4868303
9. Del Valle, J., Ramírez, J.G., Rozenberg, M.J., and Schuller, I.K., Challenges in materials and devices for resistive-switching-based neuromorphic computing, *J. Appl. Phys.,* 2018, vol. 124, paper 211 101. https://doi.org/10.1063/1.5047800
10. Zhilova, O.V., Pankov, S., Sitnikov, A.V., Kalinin, Yu.E., Kashirin, M.A., and Makagonov, V.A., Optical and electrical properties of thin-film hetero-structures of the In_2O_3–ZnO system, *Mater. Res. Express,* 2019, vol. 6, paper 086 330. https://doi.org/10.1088/2053-1591/ab2721
11. Lee, S.J., Hwang, C.S., Pi, J.E., Yang, J.H., Byun, C.W., Chu, H.Y., Cho, K.I., and Cho, S.H., High-performance amorphous multilayered ZnO–SnO_2 heterostructure thin-film transistors: fabrication and characteristics, *ETRI J,* 2015, vol. 37, pp. 1135–1142. https://doi.org/10.4218/etrij.15.0114.0743
12. Zhilova, O.V., Pankov, S.Yu., Sitnikov, A.V., Kalinin, Yu.E., Volochaev, M.N., and Makagonov, V.A., Structure and electrophysical properties of thin-film SnO_2–In_2O_3 heterostructures, *J. Mater. Sci.–Mater. Electron.,* 2019, vol. 30, pp. 11859–11867. https://doi.org/10.1007/s10854-019-01503-w
13. Cui, G., Han, D., Dong, J., Cong, Y., Zhang, X., Li, H., Yu, W., Zhang, S., Zhang, X., and Wang, Y., Effects of channel structure consisting of ZnO/Al_2O_3 multilayers on thin-film transistors fabricated by atomic layer deposition, *Jpn. J. Appl. Phys.,* 2017, vol. 56, paper 04CG03. https://doi.org/10.7567/JJAP.56.04CG03
14. Kalinin, Yu.E., Zhilova, O.V., Babkina, I.V., Sitnikov, A.V., Makagonov, V.A., and Remizova, O.I., Effect of heat treatment on the electrical properties of thin yttrium-doped In_2O_3 films, *Inorg. Mater.,* 2018, vol. 54, no. 9, pp. 936–942. https://doi.org/10.1134/S0020168518090030
15. Suchea, M., Katsarakis, N., Christoulakis, S., Nikolopoulou, S., and Kiriakidis, G., Low temperature indium oxide gas sensors, *Sens. Actuators, B,* 2006, vol. 118, pp. 135–141. https://doi.org/10.1016/j.snb.2006.04.020
16. Rylkov, V.V., Nikolaev, S.N., Chernoglazov, K.Yu., Demin, V.A., Sitnikov, A.V., Presnyakov, M.Yu., Vasiliev, A.L., Perov, N.S., Vedeneev, A.S., Kalinin, Yu.E., Tugushev, V.V., and Granovsky, A.B., Tunneling

anomalous Hall effect in nanogranular CoFe–B–Al–O films near the metal–insulator transition, *Phys. Rev. B: Condens. Matter Mater. Phys.,* 2017, vol. 95, paper 144 202.
https://doi.org/10.1103/PhysRevB.95.144202

17. Kalinin, Yu.E., Kashirin, M.A., Makagonov, V.A., Pankov, S.Yu., and Sitnikov, A.V., Properties of amorphous carbon thin films grown by ion beam sputtering, *Tech. Phys.,* 2017, vol. 62, no. 11, pp. 1724-1730.
https://doi.org/10.1134/S1063784217110123
18. Zhilova, O.V., Pankov, S.Yu., Sitnikov, A.V., Kalinin, Yu.E., and Babkina, I.V., The structure and the gas sensitive properties of the thin films of zinc oxide, *AIP Conf. Proc.,* 2017, vol. 1886, paper 020 054.
https://doi.org/10.1063/1.5002951
19. Zhilova, O.V., Pankov, S.Y., Sitnikov, A.V., Kalinin, Y.E., and Babkina, I.V., The structure and electrical properties of In_2O_3–C heterogeneous system, *AIP Conf. Proc.,* 2018, vol. 2015, paper 020 123.
https://doi.org/10.1063/1.5055196
20. Bondarenko, V.B. and Filimonov, A.V., Criterion for strong localization on a semiconductor surface in the Thomas–Fermi approximation, *Semiconductors,* 2017, vol. 51, no. 10, pp. 1321–1325.
https://doi.org/10.1134/S1063782617100062
21. Mott, N. and Davis, E., *Electronic Processes in Non-Crystalline Materials,* Oxford: Clarendon, 1979.
22. Lin, J.J. and Li, Z.Q., Electronic conduction properties of indium tin oxide: single-particle and many-body transport, *J. Phys.: Condens. Matter,* 2014, vol. 26, no. 34, paper 343 201.
https://doi.org/10.1088/0953-8984/26/34/343201
23. Suzuki K., Fuzimori, H., and Hashimoto, K., *Amorfnye metally* (Amorphous Metals), Moscow: Metallurgiya, 1987 (translated from Japanese).
24. Polyanskaya, T.A. and Shmartsev, Yu.V., Quantum correction to the conductivity of semiconductor with a two-dimensional and a 3-dimensional electron-gas. Experiments, *Phys. Tekh. Poluprovodn.,* 1989, vol. 23, no. 1, pp. 3–32.
25. Bartolomeo, D., Sarno, M., Giubileo, F., Altavilla, C., Iemmo, L., Piano, S., Bobba, F., Longobardi, M., Scarfato, A., Sannino, D., Cucolo, A.M., and Ciambelli, P., Multiwalled carbon nanotube films as small-sized temperature sensors, *J. Appl. Phys.,* 2009, vol. 105, paper 064 518.
https://doi.org/10.1063/1.3093680
26. Zhilova, O.V., Makagonov, V.A., and Pankov, S.Yu., Structure of thin films of carbon-modified In_2O_3 and ZnO wide-band-gap semiconductors, *Vestn. Voronezhsk. Gos. Tekh. Univ.,* 2018, vol. 14, no. 4, pp. 168–173.

Translated by O. Tsarev